FUPRE Journal of Scientific and Industrial Research
Vol.3, (3), 2019
ISSN: 2579-1184 (Print) ISSN: 2578-1129 (Online

Integrated Geophysical Techniques: A Viable Tool for Accentuating the Needed Importance of Side-Drains to Paved Road Networks

[1]Amadasun, C. V. O.[*]; [1]Odeh, A. I, [2]Iguisi, A. E. and [3]Usifo, A. G.
[1]Department of Physics, Faculty of Physical Sciences, Ambrose Alli University, Ekpoma.
[2]Department of Chemical Engineering, School of Engineering, Edo State Polytechnic, Usen, Edo State,
[3]Department of Physics with Electronics, Crawford University, Igbesa, Ogun State, Nigeria
***Corresponding Author (cvoamadasun@aauekpoma.edu.ng 08033772890)**

Abstract
Subsurface Geo-electrical surveys were carried out along the Uteh-Aduwawa road (popularly called the Upper Mission road extension), a suburb of Benin City but in Ikpoba-Okha Local Government Area of Edo State, in order to assess the integrity of a portion of the road that was being unused by motorists and commuters at a point in time, and to know the possible cause(s) of the seeming road failure leading to its disuse. The methodology involved the combined use of the Dipole-Dipole profiling and Vertical Electrical Sounding (VES) as well as the Electromagnetic Very Low Frequency (VLF) and the data obtained were subjected to standard best procedures involving the use of manual curve matching and further enhancement interpretations using WINRESIST and DIPROfWIN inversions software for the resistivity survey, while the EM-VLF was interpreted using the Fraser and Karous-Hjielt filtering software. The interpreted field data showed high resistivity-value subsoil and layers of competent sub-grade soil as agreed by the local geology of the area despite the fact that the entire portion of the road was submerged in flood. These strongly suggested that the road under study seemingly 'failed', not because of the earth materials used in its construction or the in-situ subsoil on which the road was constructed but basically due to the non-functionality of the side drains, either as a result of its design in terms of size, depth and elevation to cater for the volume of adjoining floods from the off-lanes or proper lack of self de-silting mechanism in its construction thereby leading to huge floods and standing 'pool of water' on the road even long after the rains were over. The resultant effect of this on the roadway is a continuous micro-detachment of bituminous overlay on the pavement.

Keywords: Integrity, non-functionality, in-situ, aggregates, accentuate.

1. Introduction

Road has been defined as an open way (generally public) for travel or transportation while its pavement is said to be a sum total of the surface course, binder course and base; or simply a combination of the surfacing and base of any road network (Amadasun, 2015), as depicted in Fig.1 below:

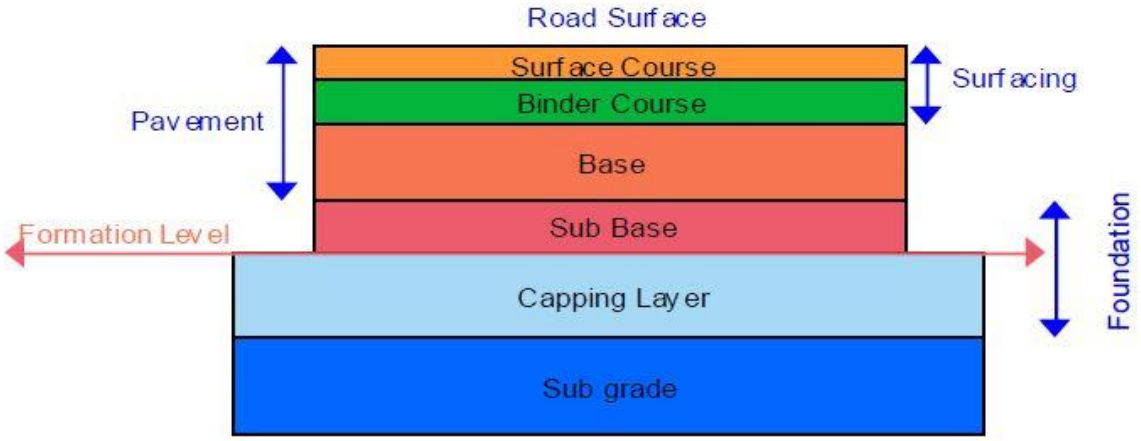

Fig.1: Road Pavement Terminology

The inability of constructed paved roads to function maximally in terms of providing pleasurable smooth driving experience, occasioned by potholes, bulges, depressions and the likes, besides the deliberate speed bumps for intended purpose(s) is referred to as road failure. Several researches have been carried on the subject matter and several factors have been adduced to be responsible for road failure. Notable amongst them but not exclusive to the following are: Onuoha and Onwuka (2014) and Aigbedion (2007), who employed shallow electromagnetic evaluation to assess the base integrity of some roads; Adegoke-Anthony and Agada (1980) and Ajayi (1987) opined that inadequate knowledge of geotechnical characteristics and behaviour of residual soils on which the roads are built and non-recognition of the influence of geology and geomorphology during the design and construction phases could be a major factor. Poor design, lack of adequate maintenance and usage to which such roads are subjected are also factors that cannot be disregarded (Jain and Kumar, 1998; TRRL, 1991; and Ibrahim, 2011). However, according to the works of Onoyan-Usina *et al*. 2013, bad drainage increases the deterioration of road pavements as the water content of the granular material increases and that even in rigid pavements, temperature gradients across the concrete slab can also initiate structural defects (Diefenderfer, 2002). The lifespan of the pavement can be greatly reduced by poor drainage and can have serious environmental impacts if left unattended to and as such, there is need to design and construct roads to allow for frequent and safe discharges of its runoffs and floods from adjoining off-lanes (McRobert *et al*., 2000). This research aimed at validating the use of geophysical technique to accentuate the needfulness of side drains for a failed road pavement adjudged to have been underlain by competent subsurface materials geologically.

2. Materials and Method

2.1 Location and Geology of Study Area

The study area is a portion of the Uteh-Aduwawa road (popularly called the Upper Mission road extension), a suburb of Benin City but in Ikpoba-Okha Local Government Area of Edo State. The road serves as a major link road between the City centre and the upper part of the City popularly referred to as the Ikpoba hill axis and a major bypass to the heavily trafficked Oregbeni-Ikpoba slope-Akpakpava road of Benin City metropolis. Geology of the study area falls under the Benin formation of the Niger delta region. Ikhile (2016) noted that the factors that characterized the Benin region as an area could best be termed as environment of weathering, which includes geological foundation rock types, types and density of plant cover, availability of readily weathered rocks, and tropical humid climate with seasonality of rainfall or alternating wet and dry seasons and topography amongst others. Reyment (1965) identified that the sedimentary basin, made up of reddish earth underlain by sands, sandy clay and ferruginized sandstone that mark the paleocoastal environment of Paleocene-pleistocene age underlie the Benin region. These sediments spread across the Southern fringes of the Anambra basin and marking the upper fancies off-flaps of the Niger Delta. Short and Stauble (1967) and Whiteman (1982) classified the Benin region as comprising the Benin formation, Alluvium, Drift/top and the Azagba-Ogwashi formation (See Fig. 2).

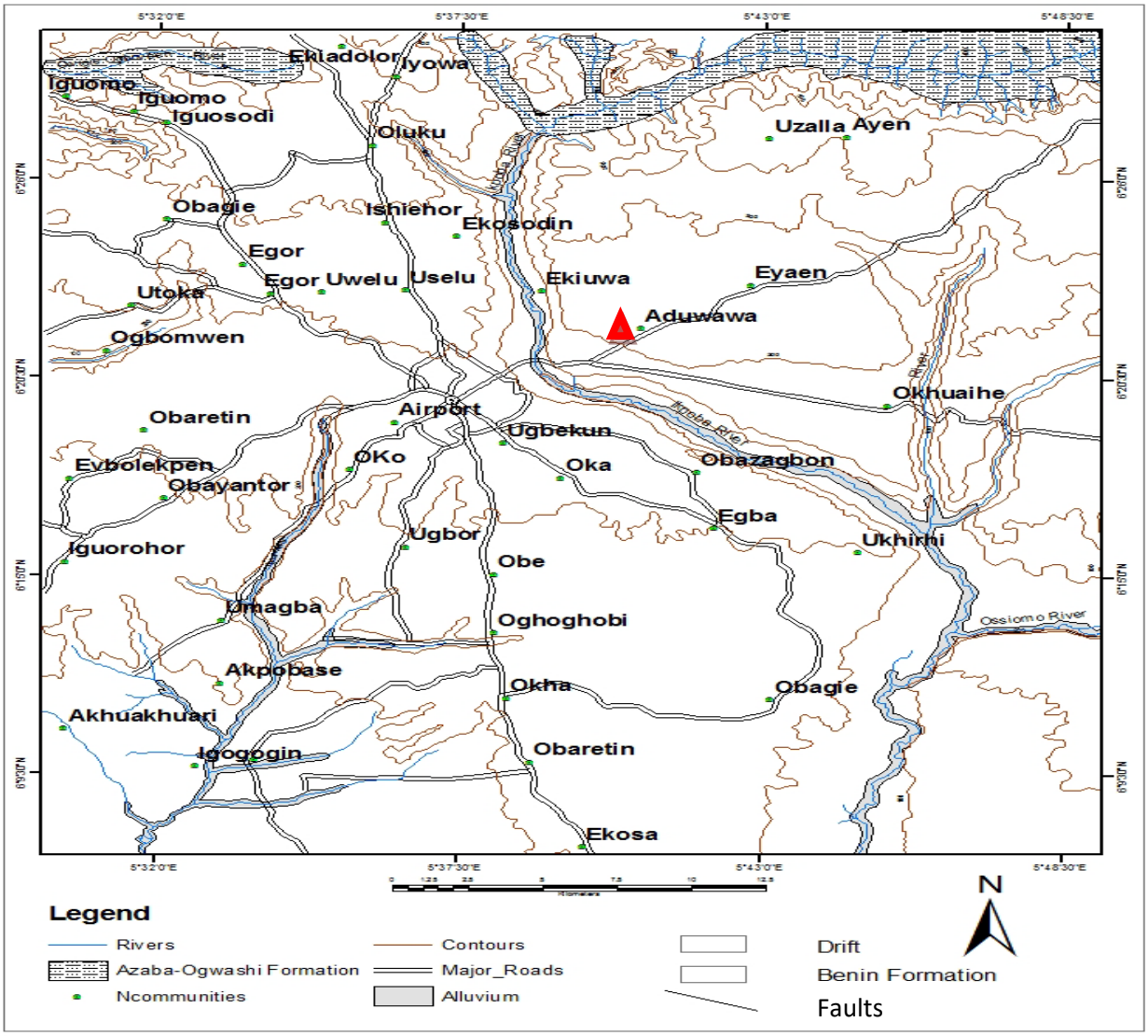

Fig. 2: Benin region geological formation with a red triangle on the location of study (Source: Akujieze, 2004)

2.2 Methodology

The methodology adopted for this study is the integrated use of Electrical resistivity and Electromagnetic methods. The Electrical profiling otherwise known as Constant Separation Traversing (CST) and the Vertical Electrical Sounding (VES) employing Dipole-dipole array and Schlumberger arrays respectively, were used for the Electrical resistivity survey. The traditional four-electrode probing (see Fig. 3 below) was done and the mathematical formulas as derived by several authors (Amadasun *et al.*, 2018):

$$V = \frac{I\rho}{2\pi r}$$

This is the fundamental relationship between/or for all prospecting from the

surface of the earth. The potential at any point due to the current flow is equal to the sum of the contributions from the individual current electrodes. The Voltage measured in a four (4) electrode survey over a homogenous ground as depicted by the fig. below is given by:

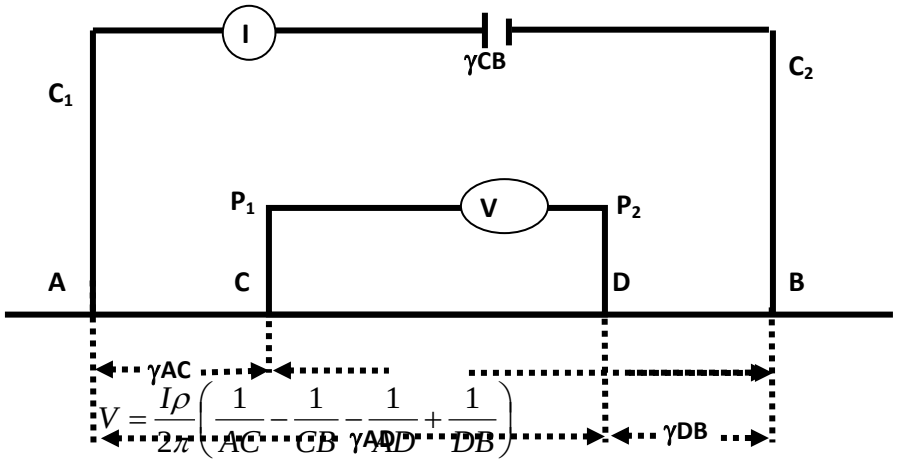

Fig. 3: General four electrode configuration for resistivity measurement, consisting of a pair of current electrodes (A, B) and a pair of potential electrodes. (C,,D)

where V is the Voltage difference between electrodes C and D due to a current I flowing in the ground. Distances from the potential electrodes to the positive and negative current electrodes are indicated by AC and DB respectively. Such that AC, for example, is the distance from Voltage electrode P_1 to the positive current electrode C_1.

Note: From Equation 2,

$$V = \frac{I\rho}{2\pi} G \qquad 3$$

which implies $\rho = \frac{2\pi V}{I} . \frac{1}{G} = K \frac{V}{I}$

where G represents the expression in brackets in equation (2) and $K = \frac{2\pi}{G}$ denotes the geometric factor of an electrode configuration.

The value of ρ determined in this way for a homogenous conducting medium is independent of the positions of electrodes and is not affected when the positions of the current and potential electrodes are interchanged (Amadasun *et al.*, 2018). The Schlumberger (Fig. 4) and Dipole-dipole (Fig. 5) configurations/arrays were calculated respectively by equations 5 and 6:

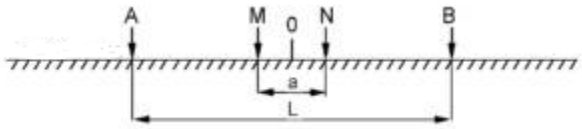

Fig. 4: Schlumberger electrode array.

$$\rho_a = \frac{\pi \Delta V}{I}\left(\frac{\left(AB/2\right)^2 - \left(MN/2\right)^2}{MN}\right)$$

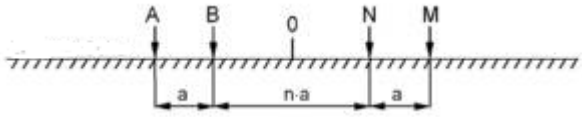

Fig. 5: Dipole-dipole electrode array.

$$\rho_a = \frac{\Delta V}{I}\pi an(n+1)(n+2)$$

The equipment used for the resistivity survey was the ABEM SAS 1000 Terrameter and its accessories.

The principle that a current flowing through a conductor produces lines of magnetic force in the form of rings about it is the basis upon which all electromagnetic methods are based. These lines of force have the same properties as those found associated with an ordinary magnet and will affect the position of a magnetic needle in the same manner. If the current (Primary current) in the conductor is alternating, the magnetic field (Primary field) associated with it will also alternate in intensity and change in direction. Now by the theory of electromagnetic induction, if a second conductor is brought within this alternating magnetic field, there will be induced in it an alternating current (Secondary current) which will have its own magnetic field (Secondary field) associated with it. This secondary electromagnetic field combines with and modifies either the: (a) direction, (b) intensity, or (c) quality of the primary electromagnetic field. This modification of the primary field may be detected and measured in a number of ways depending on the method employed. In this study using the ABEM WADI VLF meter, the Very Low Frequency (VLF) method which uses navigation signal as transmitter and operates in the low frequency range where conduction currents predominate over displacement currents, measures tilt and phase, and whose main field is horizontal. It detects electrical conductors by utilizing radio signal in the 15 to 30 KHz range that are used for military communications and compares the magnetic field of the primary signal (transmitted) to the secondary signal (induced current flow within the subsurface electrical conductor). The meter operates in the frequency domain and allows measurement of both the in-phase (or real) component and 90° out-of-phase (or quadrature/imaginary) component.

3. Results and Discussion

3.1 Presentation of Results

The data obtained from the EM-VLF, Dipole-dipole and Schlumberger surveys are presented respectively as follows:

Table 1: EM-VLF Data

Co-ordinate: 2000/0000
Spacing Interval: 10m
Frequency: 24.6 KHz
Signal Strength: 7

Station	Raw Real	Filtered Real	Raw Imaginary	Filtered Imaginary	Remark
0	0.0	9.9	6.8	-3.0	Failed
1	6.8	15.0	20.1	3.2	Failed
2	15.2	-8.4	1.7	7.9	Failed
3	-17.0	-26.1	-20.2	-9.2	Failed
4	-14.4	-7.7	36.7	-6.4	Failed
5	5.9	-17.5	15.1	15.7	Failed
6	-22.7	-24.3	-20.4	11.1	Failed
7	-2.9	-12.4	-23.8	3.8	Failed
8	-13.0	-7.9	-22.2	-1.2	Failed
9	-2.5	22.6	-16.0	-4.7	Failed
10	22.7	25.3	-6.4	-1.7	Failed
11	8.5	3.2	-12.2	1.9	Partly Failed
12	2.0	-12.2	-13.4	0.5	Partly Failed
13	-12.9	-20.9	-22.6	-9.0	Partly Failed
14	-9.6	-16.5	15.4	-11.2	Stable Portion
15	-11.0	-7.2	15.3	-0.4	Stable Portion
16	0.1	4.7	10.1	0.7	Stable Portion
17	3.8	4.0	7.1	1.2	Stable Portion
18	2.3	0.2	7.1	0.0	Stable Portion
19	-2.4	2.6	8.2	-0.5	Stable Portion
20	4.4	4.4	9.1	-0.4	Stable Portion

Table 2: Dipole-dipole Resistivity Field Record of 10m electrode spacing

C1	C2	P1	P2	K	R(Ω)	ρa(Ωm)
0	1	2	3	188.4956	1.453	273.884
		3	4	753.9822	0.3486	262.8382
		4	5	1884.9556	0.1677	316.4071
		5	6	3769.9112	0.1067	402.2495
		6	7	6597.3446	0.1494	985.6433
1	2	3	4	188.4956	0.9424	177.6383

		4	5	753.9822	0.2938	221.52
		5	6	1884.9556	0.1626	306.4938
		6	7	3769.9112	0.793	2989.5396
		7	8	6597.3446	0.8723	5754.8637
2	3	4	5	188.4956	0.6729	126.8387
		5	6	753.9822	0.2571	193.8488
		6	7	1884.9556	0.2673	503.8486
		7	8	3769.9112	0.1392	524.7716
		8	9	6597.3446	0.0992	654.4566
3	4	5	6	188.4956	1.006	189.6266
		6	7	753.9822	0.3008	226.7978
		7	8	1884.9556	0.1321	249.0026
		8	9	3769.9112	0.1484	559.4548
		9	10	6597.3446	0.1128	744.1805
4	5	6	7	188.4956	0.802	151.1735
		7	8	753.9822	0.2724	205.3848
		8	9	1884.9556	0.2134	402.2495
		9	10	3769.9112	0.19	716.2831
		10	11	6597.3446	0.0968	638.623
5	6	7	8	188.4956	0.8823	166.3097
		8	9	753.9822	0.433	326.4743
		9	10	1884.9556	0.3618	681.9769
		10	11	3769.9112	0.2144	808.269
		11	12	6597.3446	0.124	818.0707
6	7	8	9	188.4956	0.9575	180.4845
		9	10	753.9822	0.498	375.4831
		10	11	1884.9556	0.238	448.2424
		11	12	3769.9112	0.2205	831.2654
		12	13	6597.3446	0.1158	763.3982
7	8	9	10	188.4956	0.6424	121.0896
		10	11	753.9822	0.3212	242.1791
		11	12	1884.9556	0.1565	294.9956
		12	13	3769.9112	0.0771	290.6602
		13	14	6597.3446	0.076	501.3982

8	9	10	11	188.4956	0.9809	184.8953
		11	12	753.9822	0.4543	342.5341
		12	13	1884.9556	0.2541	478.9672
		13	14	3769.9112	0.1626	612.9876
		14	15	6597.3446	0.0864	570.0106
9	10	11	12	188.4956	1.82	343.062
		12	13	753.9822	1.647	1241.8087
		13	14	1884.9556	0.6556	1235.7769
		14	15	3769.9112	0.245	923.6282
		15	16	6597.3446	0.292	1926.4246
10	11	12	13	188.4956	1.301	245.2328
		13	14	753.9822	1.199	904.0247
		14	15	1884.9556	1.473	2776.5396
		15	16	3769.9112	0.039	148.9115
		16	17	6597.3446	0.557	3074.7209
11	12	13	14	188.4956	0.792	149.2885
		14	15	753.9822	0.2876	216.8453
		15	16	1884.9556	0.1534	289.1522
		16	17	3769.9112	0.1189	448.2424
		17	18	6597.3446	0.0984	649.1787
12	13	14	15	188.4956	0.7827	147.5355
		15	16	753.9822	0.3029	228.3812
		16	17	1884.9556	0.2063	388.8663
		17	18	3769.9112	0.1128	425.246
13	14	15	16	188.4956	0.7969	150.2121
		16	17	753.9822	0.3121	235.3178
		17	18	1884.9556	0.1433	270.6467
14	15	16	17	188.4956	0.7888	148.6853
		17	18	753.9822	0.2754	207.1141
15	16	17	18	188.4956	0.93	175.3009

Table 3: VES 1 Field Data Using the Schlumberger Array

Electrode position	Current Electrode Position (m) (AB/2)	Potential Electrode Position (m) MN/2	Geometric Factor K	Resistance (Ω)	ρa (Ωm)
1	1	0.5	6.28	43.92	275.8176
2	2	0.5	25.13	16.47	413.8911
3	3	0.5	56.55	8.18	462.579
4	4	0.5	100.53	4.76	478.5228
5	6	0.5	226.19	1.647	372.5349
6	6	1	113.1	3.314	374.8134
7	8	1	201.16	1.819	365.7281
8	12	1	452.39	0.8735	395.1627
9	15	1	706.86	0.5618	397.1139
10	15	2	353.43	1.321	466.881
11	25	2	981.75	0.7869	772.5391
12	32	2	1608.5	0.6232	1002.41
13	40	2	2513.27	0.5256	1320.9747
14	40	5	1005.31	1.128	1133.9897

Table 4: VES 2 Using the Schlumberger Array

Electrode position	Current Electrode Position (m) (AB/2)	Potential Electrode Position (m) MN/2	Geometric Factor K	Resistance (Ω)	ρa (Ωm)
1	1	0.5	6.28	64.15	402.862
2	2	0.5	25.13	13.41	336.9933
3	3	0.5	56.55	5.712	323.0136
4	4	0.5	100.53	3.689	370.8552
5	6	0.5	226.19	1.86	420.7134
6	6	1	113.1	4.229	478.2999

7	8	1	201.16	2.297	461.8348
8	12	1	452.39	1.138	514.8198
9	15	1	706.86	0.733	518.1284
10	15	2	353.43	1.159	409.6254
11	25	2	981.75	0.7137	700.675
12	32	2	1608.5	0.5754	925.5309
13	40	2	2513.27	0.2816	707.7368
14	40	5	1005.31	0.6649	668.4306

The data above were processed according to standard procedures and the following results are displayed in likewise/sequential manner:

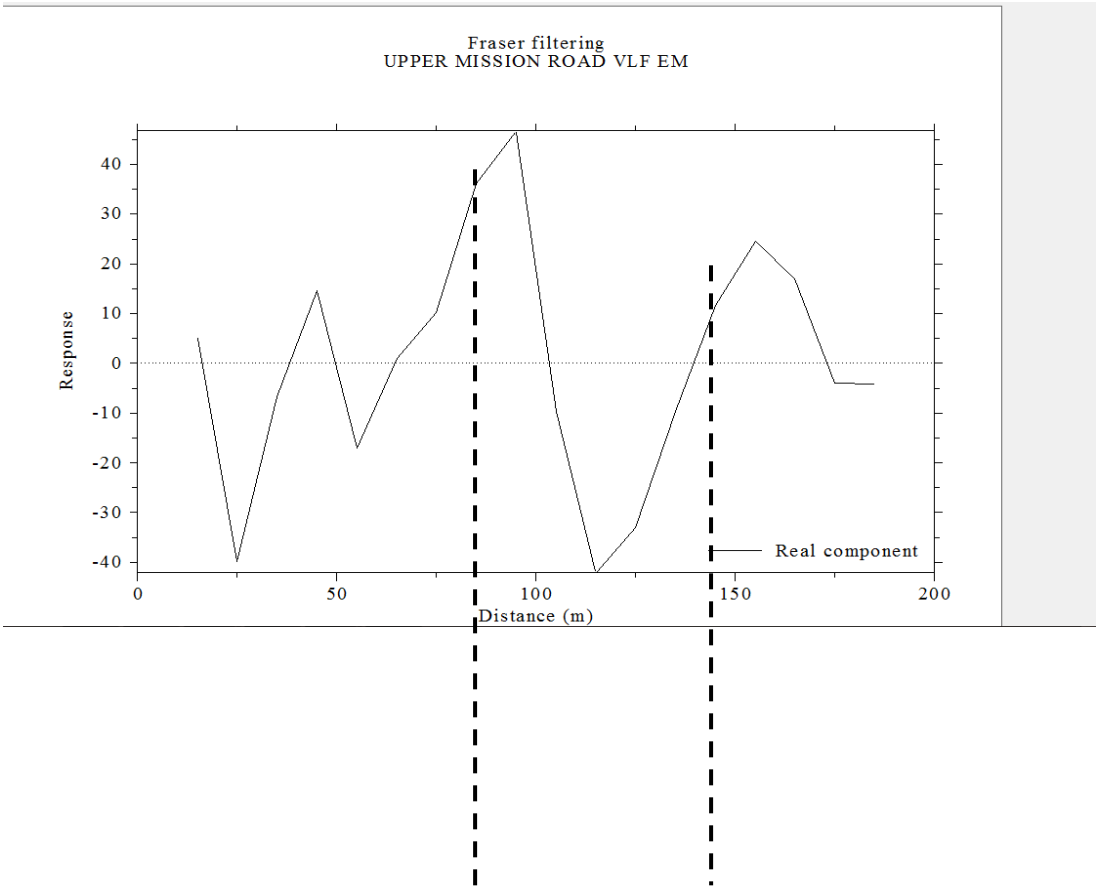

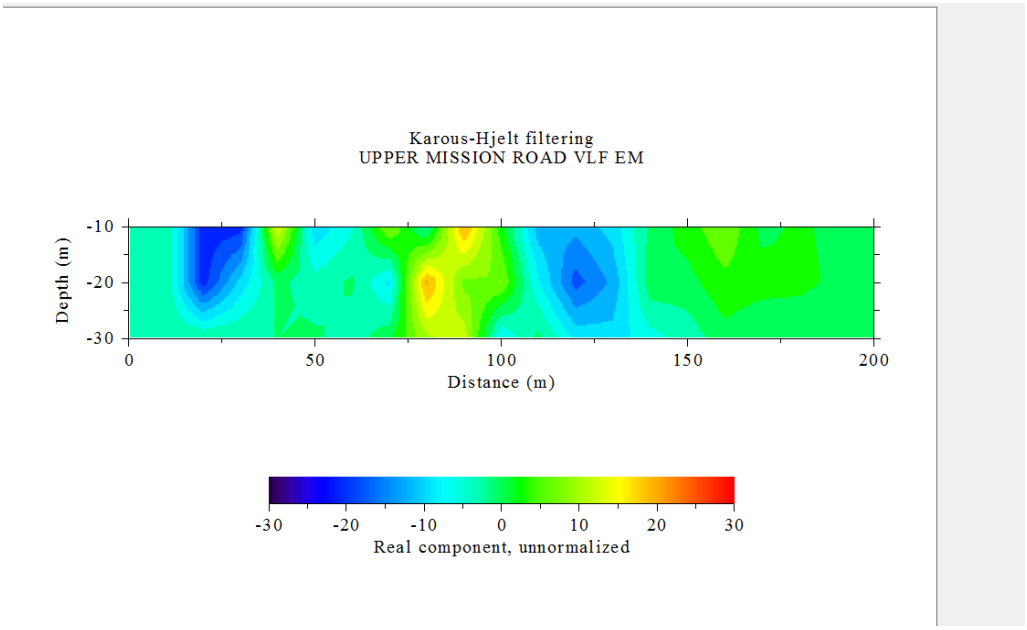

Fig. 6: Fraser and Karous-Hjelt processed EM-VLF data.

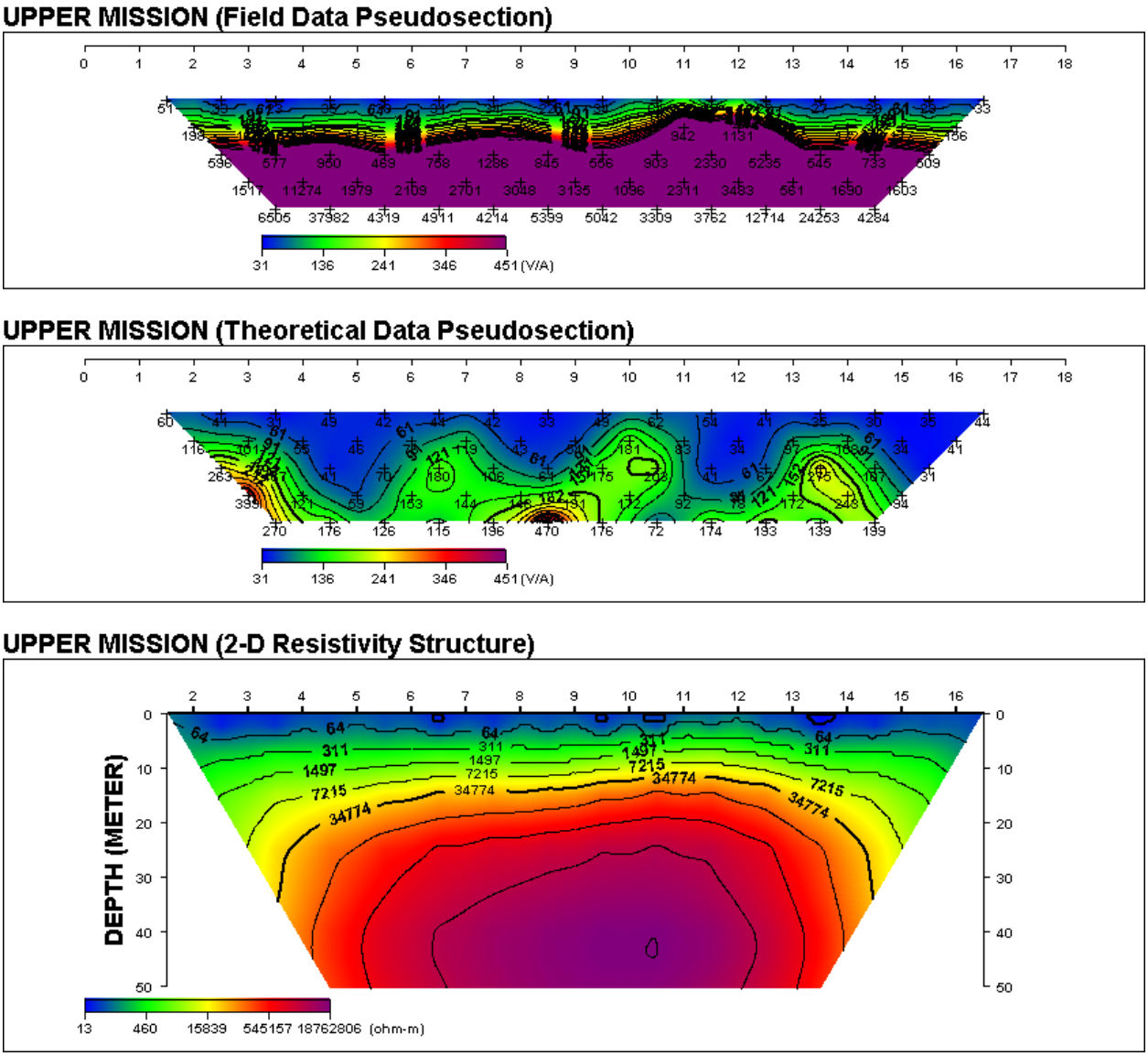

Fig. 7: Dipole-dipole processed data using DIPROfWIN.

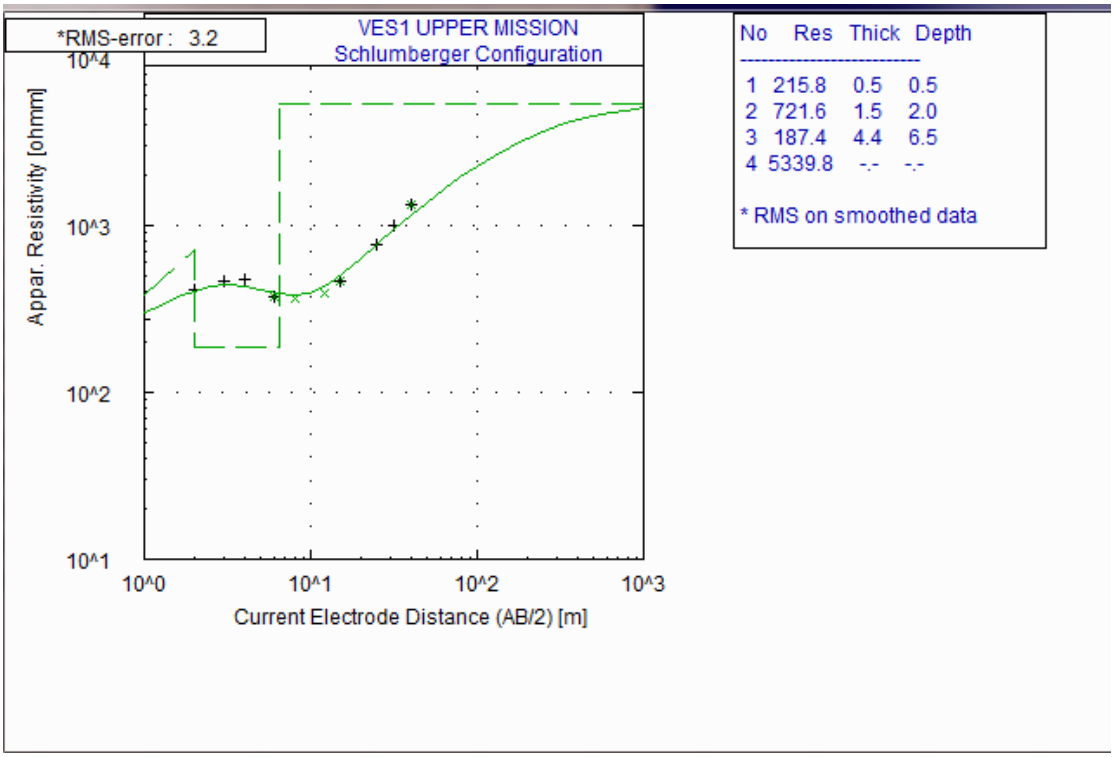

Fig. 8: VES 1 processed data using WINRESIST.

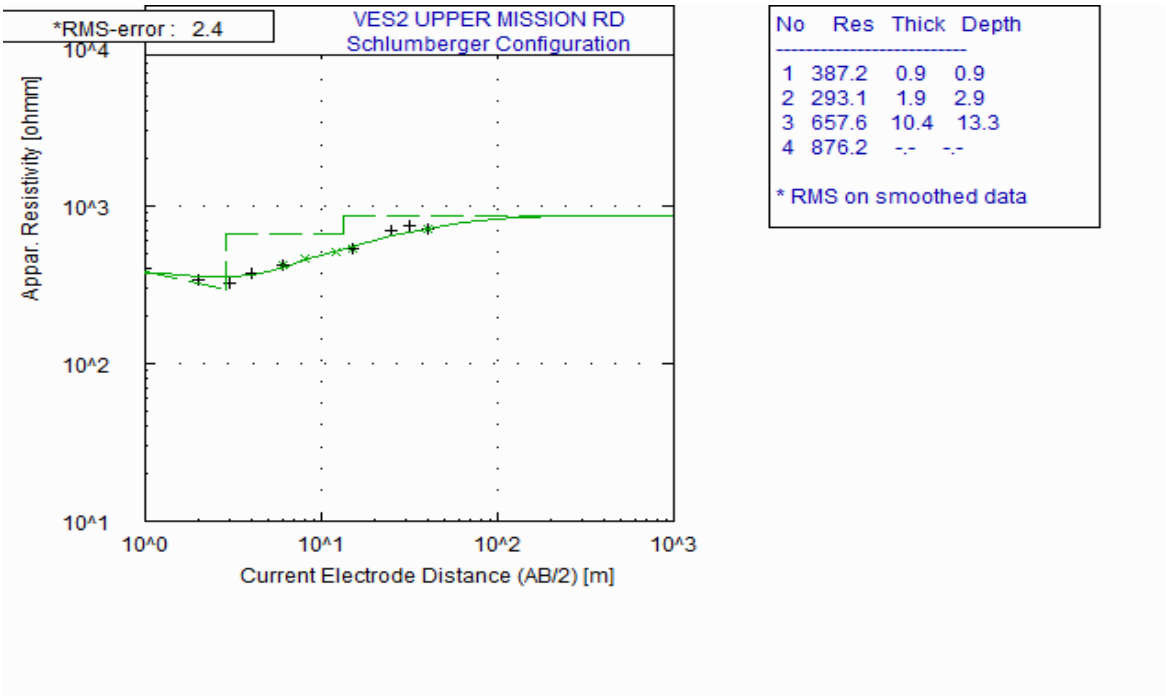

Fig. 9: VES 2 processed data using WINRESIST.

3.2 Discussion of Results

First, the Raw Real and Filtered Real data were plotted simultaneously against the distance to obtain a signature, with further processing using the Fraser filtering before subjecting it to the Karous-Hjelt (K-H) filtering. The various amplitudes shown by the peaks at about 95m and 155m, indicate conductivity changes in the near subsurface. On the K-H pseudo-section, the yellow colour indicates the conductive bodies which coincide with the high amplitude anomaly on the profile above as shown by the broken lines in Fig. 6.

The 2-D resistivity structure observed upon subjecting the Dipole-dipole data to the DIPROfWIN software showed a subsurface of varying resistivities at varying depths. First, we observed the overlying water and its consequent flooded top soil of about 0-4m, followed by a high resistivity earth material and a higher one in that order, as seen in Fig. 7.

The sounding curves of the two VES's (VES 1 and VES 2) conducted at the two peaks observed from the Fraser filtering at about 95m and 155m are classified as KH ($\rho_1<\rho_2>\rho_3<\rho_4$) and HA ($\rho_1>\rho_2<\rho_3<\rho_4$) curve types. The quantitative interpretation of the geo-sounding curves by partial curve matching and computer iteration techniques revealed four (4) geo-electric layers based on characteristic resistivity ranges. VES 1 (Fig. 8) showed a top soil of about 0.5m thickness, with two other successive layers of suspected sandstone and laterite (totaling about 6.5m thickness) followed by weathered formation; while VES 2 (Fig. 9) showed a top soil of 0.9m thickness, suspected laterite of 0.9m thickness, followed by a third layer of sandstone of 10.4m thickness, underlain by another layer of suspected weathered formation at a depth of about 13m.

Conclusion

From the analysis of the three approaches adopted, the interpreted field data showed high resistivity-value subsoil and layers of competent sub-grade soil as agreed by the local geology of the area despite the fact that the entire portion of the road was submerged in flood. These strongly suggested that the road under study seemingly 'failed', not because of the incompetence of the earth materials used in its construction or the in-situ subsoil on which the road was constructed as the 2-D resistivity structure or inversed model of the Dipole-dipole pseudo-section revealed a uniformed competent layers of earth's materials beneath the flooded topsoil down to the fresh bedrock, a confirmation of the paved work done on it prior to its earlier construction, which was also buttressed by the model parameters of the VES's, but basically due to the non-functionality of the side drains, either as a result of its design in terms of size, depth and elevation to cater for the volume of adjoining floods from the off-lanes or lack of proper self de-silting mechanism in its construction thereby leading to huge floods and standing 'pool of water' on the road

even long after the rains were over. The resultant effect of this on the roadway is a continuous micro-detachment of bituminous overlay on the pavement which further degrades to the stripping of the asphalt lay from its aggregates and by continuous flooding, these are relocated and the sub-grade soil is exposed.

On recommendation, it is advised that emphasis should be channeled to proper drainage, either by way of design, de-silting of the existing side drains or outright reconstruction of formidable drainage system to cater for the run-offs to avoid stagnancy and ease accessibility.

References

Adegoke-Anthony, W. C. and Agada, O. A., (1980). Geotechnical Characteristics of Some Residual Soils and their Implications on Road Design in Nigeria. Technical Lecture. Lagos, Nigeria, pp.1-16.

Aigbedion, I., (2007). Geophysical Investigation of Road Failure Using Electromagnetic Profiles Along Opoji, Uwenlenbo and Illeh in Ekpoma-Nigeria. *Middle-East Journal of Scientific Research*, 2 (3 & 4):111-115.

Ajayi, L. A., (1987). Thought on Road Failures in Nigeria. *The Nigerian Engineer*, 22 (1):10-17.

Akujieze, C. N., (2004). Effects of Anthropogenic Activities (Sand Quarrying and Waste Disposal) on Urban Groundwater System and Aquifer Vulnerability Assessment in Benin City, Edo State, Nigeria. Ph.D Thesis, University of Benin, Benin City, Nigeria.

Amadasun, C.V.O.; Jegede, S.I. and Iyoha, A., (2015). Optimizing Geophysical Tomographic Approaches in Road Failure of the Ozalla-Uhunmora Road, Near the Agor-Igbirra Settlement, In Owan West Local Government Area of Edo State. *Nigerian Annals of Natural Science*, 15 (1): 122-130.

Amadasun, C. V. O; Odeh, A. I. and Iguisi, A. E., (2018). Use of Integrated Geophysical Methods for Linear Assessment of a Portion of Siluko Road in Egor Local Government Area of Edo State, Nigeria. *Journal of Physical and Applied Sciences*, 1 (1): 117-134.

Diefenderfer, B. K., (2002). Moisture Content Determination and Temperature Profile Modeling of Flexible Pavement Structures. Ph.D Thesis. Faculty of the Virginia Polytechnic Institute and State University.

Ibrahim, K., (2011). Nigerian Roads Need N70 Billion for Repairs Annually. Daily Times. Article. May 30, 2011 - 10:23am . http://dailytimes.com.ng/article/nigerian-roads-need-N70-billion-repairs-annually.

Ikhile, I. C., (2016). Geomorphology and Hydrology of the Benin Region, Edo State, Nigeria. *International Journal of Geosciences*, 7: 144-157.

Jain, S. S. and Kumar, P., (1998). Report on Causes of Cracks Occurrence in Ramghat - Aligarh Road in U.P. Report Submitted to PWD, Aligarh.

McRobert, J.; Robinson, P. and Giummarra, G., (2000). Environmental Best Practice for Outback Roads-Guidelines only for Transport SA RC 90165-4.

Onoyan-Usina, A; Lazhi, Y. G. and Itomi-Ushi, D. P., (2013). Bad Drainage and its Effect on Road Pavement Conditions in Nigeria. *Civil and Environmental Research*, 3(10):7-15.

Onuoha, D. C. and Onwuka, S. U., (2014). The Place of Soil Geotechnical Characteristics in Road Failure: A study of the Onitsha-Enugu Expressway, Southeastern Nigeria. *Civil and Environmental Research*, 6 (1): 55-67.

Reyment, R. A. (1965). *Aspects of the Geology of Nigeria*. Ibadan University Press, Ibadan.

Short, K. C. and Stauble, A. J. (1967). Outline of the Geology of Onitsha, Owerri and Benue Provinces. Geological Survey of Nigeria, Bulletin No.21.

Transport Road Research Laboratory (TRRL). (1991): Maintenance Techniques for District Engineers, Vol. 2, TRRL. Crow Thorne England.

Whiteman, A. J. (1982). *Nigeria: Its Petroleum Geology, Resources and Potential, 1 & 2*. Graham and Turtman Limited, London, pp: 26-110.